School of Mathematical
and Physical Sciences

University of Reading

Department of Mathematics and Statistics

Preprint MPS-2013-11

1 October 2013

Implementation of an Interior Point Source in the Ultra Weak Variational Formulation through Source Extraction

by

C.J. Howarth, P.N. Childs and A. Moiola

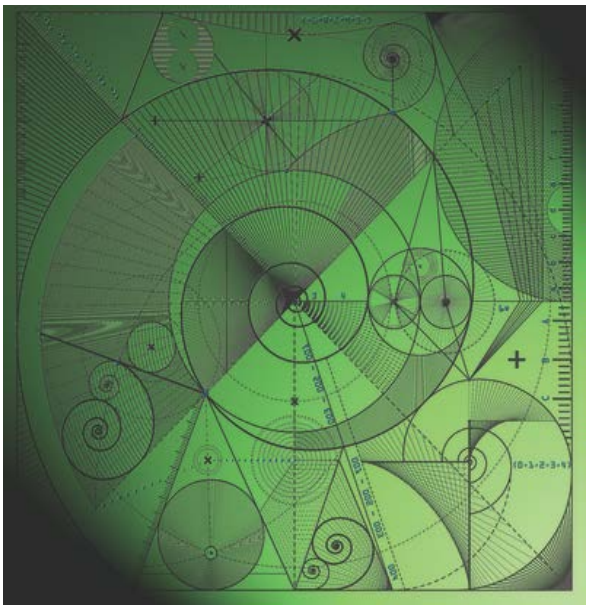

Implementation of an Interior Point Source in the Ultra Weak Variational Formulation through Source Extraction

C. J. Howarth[1,*], P. N. Childs[2], A. Moiola[1]

[1] Department of Mathematics and Statistics, University of Reading, Whiteknights PO Box 220, Reading RG6 6AX, UK

[2] Schlumberger Gould Research, Cambridge, UK

*Email: charlottahowarth@googlemail.com

October 1, 2013

Abstract

The Ultra Weak Variational Formulation (UWVF) is a powerful numerical method for the approximation of acoustic, elastic and electromagnetic waves in the time-harmonic regime. The use of Trefftz-type basis functions incorporates the known wave-like behaviour of the solution in the discrete space, allowing large reductions in the required number of degrees of freedom for a given accuracy, when compared to standard finite element methods. However, the UWVF is not well disposed to the accurate approximation of singular sources in the interior of the computational domain. We propose an adjustment to the UWVF for seismic imaging applications, which we call the Source Extraction UWVF. Differing fields are solved for in subdomains around the source, and matched on the inter-domain boundaries. Numerical results are presented for a domain of constant wavenumber and for a domain of varying sound speed in a model used for seismic imaging.

Keywords: Ultra Weak Variational Formulation, Trefftz method, Helmholtz equation, time-harmonic acoustic waves, source extraction, interior point source, Hankel basis, Marmousi model.

AMS subject classification: 65N30, 35J05.

1 Introduction

The Ultra Weak Variational Formulation (UWVF), originally proposed by Cessenat and Després in [4, 5], is a new-generation finite element method for the accurate simulation of time-harmonic acoustic, elastic, and electromagnetic waves. The area of time-harmonic wave scattering is a subject of much research, with applications in seismology, medical imaging, and radar imaging.

We consider acoustic wave propagation, modelled in two dimensions by the following Helmholtz boundary value problem (BVP):

$$\nabla \cdot \left(\frac{1}{\rho}\nabla u\right) + \frac{\kappa^2}{\rho}u = f \qquad \text{in } \Omega, \tag{1a}$$

$$\left(\frac{1}{\rho}\frac{\partial u}{\partial n} - \mathrm{i}\sigma u\right) = Q\left(-\frac{1}{\rho}\frac{\partial u}{\partial n} - \mathrm{i}\sigma u\right) + g \qquad \text{on } \Gamma. \tag{1b}$$

Here $\Omega \subset \mathbb{R}^2$ is a bounded domain with Lipschitz boundary Γ; the density $\rho(\mathbf{x})$ and the wavenumber $\kappa(\mathbf{x})$ are real positive and may vary throughout the domain. The coupling parameter σ is real and positive, and f and g are the volume and boundary source terms respectively. The parameter $Q \in \mathbb{C}$, $|Q| \leq 1$, allows different types of boundary conditions: $Q = 1$, -1 and 0 correspond to Neumann, Dirichlet, and impedance boundary conditions, respectively.

The UWVF is a Trefftz-type method: the exact solution of a Helmholtz boundary value problem is approximated by a linear combination of basis functions that, inside each mesh element, are solutions of the homogeneous Helmholtz equation, i.e. equation (1a) with right-hand side $f = 0$. By incorporating information on the oscillatory behaviour of Helmholtz solutions into the approximation space, the UWVF can produce accurate results requiring significantly fewer degrees of freedom than standard finite element methods, in some cases for mesh sizes encompassing several wavelengths λ.

The solution of the Helmholtz equation is often approximated using a plane wave basis [3–5,7,9,11]; however, it is also possible to use other solutions of the homogeneous Helmholtz equation, such as a Fourier–Bessel functions as in [13].

As with standard finite element methods (FEM), the domain Ω is partitioned into a polygonal mesh; however the solution variables are impedance traces $\frac{1}{\rho}\frac{\partial u}{\partial n} - \mathrm{i}\sigma u$ on the skeleton of the mesh. These traces are approximated by the corresponding traces of a Trefftz trial space and the approximation is automatically achieved also in the element interiors if the discretised BVP is homogeneous ($f = 0$), see [3, Theorem 4.1], [10, Theorem 4.5]. In [3, 6, 7, 9]

the UWVF has been shown to be a discontinuous Galerkin (DG) method with Trefftz basis functions, allowing a simpler and more general derivation of the formulation (see e.g. [9, §3.2]) and a more straightforward error analysis.

In seismic imaging applications, point sources (monopoles or dipoles) are used in the interior of the domain, for example to represent an explosive sound source. Modelling this situation requires solving the inhomogeneous Helmholtz equation for a non-zero and singular source term f, for example a Dirac delta function. To date, the use of the UWVF to solve the inhomogeneous form of the Helmholtz equation has not received a great deal of attention in the literature: typically, sources in the exterior of the domain have been simulated by imposing non-zero boundary conditions in BVPs for the homogeneous Helmholtz equation, in order to demonstrate superior approximation properties of Trefftz methods.

In [4–7] the UWVF with non-zero source term f has been investigated, and both a priori analysis and numerical experiments have been presented. Loeser and Witzigman [12] use UWVF to solve the Helmholtz equation (1a) with a source term $f = 1$ in Ω^S and $f = 0$ elsewhere, for an active region $\Omega^S \subset \Omega$. The UWVF solution is found in the source-free region $\Omega \setminus \Omega^S$ only, after which, in an additional post-processing step, a standard finite element method (FEM) is used in the active region where f is non-zero. In practice, [12] suggests that the FEM mesh size in the active region should be no larger than $\lambda/30$, where λ is the problem wavelength, leading to a potentially computationally expensive scheme.

Here, we investigate the applicability of the UWVF to seismic imaging by considering the typical situation of an interior point source. We first consider a domain of constant wave speed, and then extend our investigations to the simulation of wave propagation through a layered velocity profile. We present a simple yet accurate method to augment the UWVF in the case of a localised non-zero source term f, which we call the Source Extraction UWVF. In this approach, the domain Ω is split into two regions: an inner source region containing the source, and an outer region comprising the remainder of the domain. In the inner region, a particular radiating solution of the inhomogeneous Helmholtz equation with source f is subtracted from the field, so that the remainder of the wavefield is amenable to a Trefftz approximation in the interior (this remainder is the wavefield which is back-scattered from the outer region into the inner region). In the outer region we solve for the total field. The solutions in the two regions are matched by prescribing the jumps of the impedance and the conjugate-impedance traces across element boundaries. If we consider a point source (a Dirac delta), then we subtract the fundamental solution in the source region. However the method can be easily generalised to other forms of sources, such as for a dipole source. A related

approach based on splitting of outgoing and back-scattered fields is used in [2, 17] for finite difference methods in time domain. A similar approach for the UWVF has been derived separately by Gabard in [6, Section 5.1] for a system of linear hyperbolic equations, applied with accurate results to the linearised Euler equations.

Details of the UWVF are given in Section 2, with explanation given as to why solving the inhomogeneous form of the Helmholtz equation poses challenges for the numerical method. In Section 3 we present the new adjustment of the UWVF for the representation of an interior point source. Accurate results for a domain with constant wavenumber are presented in Section 4, followed by results for a domain with a varying sound speed profile. The sound speed profile for the latter case is taken from a synthetic 2D acoustic model often used as a test case in seismic inversion, the Marmousi model (see [1, 15] for example).

2 The ultra weak variational formulation of the inhomogeneous Helmholtz problem

We introduce in this section the classic UWVF for the inhomogeneous Helmholtz BVP (1), which is slightly more general than that considered in [5] in the fact that varying coefficients are allowed (compare also with [11]). We mainly follow the notation of [11].

We partition Ω into a mesh $\mathcal{T} = \{\Omega_k\}_{k=1}^K$ composed of triangular elements Ω_k. We denote the boundary of an element by $\partial\Omega_k$, the inter-element boundaries by $\Sigma_{k,j} := \partial\Omega_k \cap \partial\Omega_j$, and the edges on the outer boundary by $\Gamma_k := \partial\Omega_k \cap \Gamma$. The outward pointing unit normal vector on $\partial\Omega_k$ is denoted $\mathbf{n}_k$. The wavenumber and density are assumed to be constant on each element, so piecewise constant in Ω, with $\kappa_k := \kappa|_{\Omega_k}$ and $\rho_k := \rho|_{\Omega_k}$. As in [11], on the inter-element boundaries, the parameter σ is defined as

$$\sigma := \frac{1}{2}\left(\frac{\kappa_k}{\rho_k} + \frac{\kappa_j}{\rho_j}\right) \qquad \text{on } \Sigma_{k,j};$$

on exterior edges we assume

$$\sigma := \frac{\kappa_k}{\rho_k} \qquad \text{on } \Gamma_k.$$

We introduce the Trefftz space $H := \prod_{k=1}^K H_k$, with

$$H_k := \left\{ v_k \in H^1(\Omega_k),\ -\nabla\cdot\left(\frac{1}{\rho_k}\nabla v_k\right) - \frac{\kappa^2}{\rho}_k v_k = 0 \text{ in } \Omega_k,\ \frac{\partial v_k}{\partial n_k} \in L^2(\partial\Omega_k)\right\},$$

and we represent any $v \in H$ as a vector $\{v_k\}_{k=1}^K$ with $v_k := v|_{\Omega_k}$. To avoid technical difficulties with the regularity of f and the solution u of the BVP (1), as in [4, Section I.5.1], we start by assuming that u belongs to

$$\widetilde{H} := \prod_{k=1}^{K} \widetilde{H}_k \qquad \text{with} \qquad \widetilde{H}_k := \left\{ v_k \in H^1(\Omega_k), \frac{\partial v_k}{\partial n_k} \in L^2(\partial\Omega_k) \right\}.$$

If ρ is constant and $f \in H^{-1}(\Omega)$, this is always guaranteed, otherwise $f|_{\Omega_k} \notin H^{-1}(\Omega)$ implies $u_k \notin H^1(\Omega_k)$ (for example, if f is a Dirac delta), and a discontinuous ρ may prevent u_k from belonging to $H^{3/2+\epsilon}(\Omega_k)$ for any $\epsilon > 0$ and its impedance trace from belonging to $L^2(\partial\Omega_k)$.

We define the sesquilinear forms $d, c : \widetilde{H} \times \widetilde{H} \to \mathbb{C}$ as

$$\begin{aligned} d(v,w) &:= \sum_{k=1}^{K} \int_{\partial\Omega_k} \frac{1}{\sigma} \left(-\frac{1}{\rho_k} \frac{\partial}{\partial n_k} - \mathrm{i}\sigma \right) v_k \overline{\left(-\frac{1}{\rho_k} \frac{\partial}{\partial n_k} - \mathrm{i}\sigma \right) w_k} \, \mathrm{d}S, \\ c(v,w) &:= \sum_{\substack{k,j=1 \\ k \neq j}}^{K} \int_{\Sigma_{k,j}} \frac{1}{\sigma} \left(-\frac{1}{\rho_j} \frac{\partial}{\partial n_j} - \mathrm{i}\sigma \right) v_j \overline{\left(\frac{1}{\rho_k} \frac{\partial}{\partial n_k} - \mathrm{i}\sigma \right) w_k} \, \mathrm{d}S \\ &\quad + \sum_{k=1}^{K} \int_{\Gamma_k} \frac{Q}{\sigma} \left(-\frac{1}{\rho_k} \frac{\partial}{\partial n_k} - \mathrm{i}\sigma \right) v_k \overline{\left(\frac{1}{\rho_k} \frac{\partial}{\partial n_k} - \mathrm{i}\sigma \right) w_k} \, \mathrm{d}S. \end{aligned} \tag{2}$$

In [5, Theorem 1.3] it is proved that, if $|Q| < 1$ (to ensure well-posedness), ρ and κ are constant, $f \in L^2(\Omega)$ and $g \in L^2(\Gamma)$, then the solution u of the BVP (1) satisfies the variational problem

$$d(u,v) - c(u,v) = -2\mathrm{i} \sum_{k=1}^{K} \int_{\Omega_k} f \overline{v_k} \, \mathrm{d}V + \sum_{k=1}^{K} \int_{\Gamma_k} \frac{g}{\sigma} \overline{\left(\frac{1}{\rho_k} \frac{\partial v_k}{\partial n_k} - \mathrm{i}\sigma v_k \right)} \, \mathrm{d}S \tag{3}$$

for all $v \in H$. The same proof (see also [11, Equation (10)]) holds true also for discontinuous coefficients (recall that we assumed $u \in \widetilde{H}$).

We recall that the formulation (3) and the sesquilinear forms (2) were derived in [5, Theorem 1.3] for the case of constant coefficients by summing over $\Omega_k \in \mathcal{T}$ the identity

$$\begin{aligned} &\int_{\partial\Omega_k} \frac{1}{\sigma} \left(-\frac{1}{\rho_k} \frac{\partial}{\partial n_k} - \mathrm{i}\sigma \right) u_k \overline{\left(-\frac{1}{\rho_k} \frac{\partial}{\partial n_k} - \mathrm{i}\sigma \right) v_k} \, \mathrm{d}S \\ &- \int_{\partial\Omega_k} \underbrace{\frac{1}{\sigma} \left(\frac{1}{\rho_k} \frac{\partial}{\partial n_k} - \mathrm{i}\sigma \right) u_k}_{=:A_k} \overline{\left(\frac{1}{\rho_k} \frac{\partial}{\partial n_k} - \mathrm{i}\sigma \right) v_k} \, \mathrm{d}S \end{aligned}$$

$$= 2\mathrm{i}\int_{\partial\Omega_k}\frac{1}{\rho_k}\left(u_k\overline{\frac{\partial v_k}{\partial n_k}}-\frac{\partial u_k}{\partial n_k}\overline{v_k}\right)\mathrm{d}S=-2\mathrm{i}\int_{\Omega_k}f\overline{v_k}\,\mathrm{d}V, \qquad (4)$$

which holds for all $v\in H$ and for $u\in\widetilde{H}$ solution of (1a), and substituting the term denoted by A_k with the corresponding trace from the neighbouring element or from the boundary condition. Note that complex wavenumbers κ (i.e. absorbing media) can be considered as in [3, Section 5].

The usual UWVF discretisation consists in restricting the variational problem (3) to the discrete space $H_h=\prod_{k=1}^{K}\operatorname{span}\{\phi_{k,l}\}_{l=1}^{p_k}\subset H$ defined by the basis functions $\phi_{k,l}\in H_k$, $1\le k\le K$, $1\le l\le p_k$, where p_k is the number of degrees of freedom located in Ω_k and may vary in different elements.

When solving the homogeneous Helmholtz equation, all of the integrals in (3) are defined on the element boundaries (as $f\equiv 0$ the only volume integral in (3) vanishes). On the other hand, in the general case the right-hand side of (3) includes an integral over all the elements where the source term f is non zero (or point evaluations if f is a linear combination of point sources).

A standard choice of the Trefftz basis functions $\phi_{k,l}$, i.e. equispaced plane waves or circular waves (Fourier–Bessel functions), allows high orders of approximation in the elements where $f=0$; see [16]. On the contrary, when $f\neq 0$ inside Ω_k, Trefftz functions lose their approximation properties. The use of plane waves in the inhomogeneous case can provide the same approximation of u as piecewise-linear polynomials only; this is supported by numerical experiments that found moderately high orders of convergence for the approximation of u on the skeleton of the mesh but only linear order in the meshsize h for the volume error measured in the $L^2(\Omega)$-norm, see [5, Tables 3.3 and 3.4] and [7, Section 5].

These two reasons, the integration on the mesh skeleton only and the higher orders of approximation, motivated the investigation of the UWVF in the homogeneous case, and not much effort has been devoted to the source case. If the UWVF is to be used in more general problems that may practically arise in seismic imaging, this situation needs to be tackled. In the next section we propose a modified formulation to extend the advantages of the UWVF to the special case of point sources.

3 The Source Extraction UWVF

We wish to solve the inhomogeneous Helmholtz BVP (1) in the domain Ω, when the source term f is a point source:

$$f(\mathbf{x})=-\delta(\mathbf{x}-\mathbf{x}_0), \qquad \mathbf{x}\in\Omega, \qquad (5)$$

where δ is the Dirac delta function and $\mathbf{x}_0 \in \Omega$. In this case, the right-hand side of the UWVF formulation (3) becomes $\int_{\Omega_k} f\overline{v_k}\,\mathrm{d}V = -\overline{v_k}(\mathbf{x}_0)$; $f \notin L^2(\Omega)$ and $u \notin H^1(\Omega)$. As it might be expected, numerical tests using the formulation (3) proved extremely inaccurate at representing the source, with high errors in the element containing $\mathbf{x}_0$; numerical experiments for this case are provided in Section 4.1.

In order to introduce a modified formulation, we now fix some notation. We split the domain in two open regions Ω^S and Ω^E, $\Omega = \Omega^S \cup \Omega^E \cup \Gamma^S$ where $\Gamma^S = \partial\Omega^S$ (as illustrated in Figure 1) such that the two regions correspond to a partition of the mesh: $\mathcal{T} = \mathcal{T}^S \cup \mathcal{T}^E$ with $\Omega_k \in \mathcal{T}^S$ if $\Omega_k \subset \Omega^S$ and $\Omega_{k'} \in \mathcal{T}^E$ if $\Omega_{k'} \subset \Omega^E$. On Γ^S, we denote by $\mathbf{n}_S$ the unit normal vector outward pointing from Ω^S, and set $\mathbf{n}_E = -\mathbf{n}_S$. Moreover, we require: $\mathbf{x}_0 \in \Omega_k$ for some $\Omega_k \in \mathcal{T}^S$ (thus the source is located in Ω^S and it does not lie on the mesh skeleton); the physical parameters are assumed to be constant in Ω^S, i.e. $\rho_k(\mathbf{x}) = \rho^S$ and $\kappa(\mathbf{x}) = \kappa^S$ for all $\mathbf{x} \in \Omega^S$; and $\overline{\Omega^S}$ to lie in the interior of Ω, i.e. $\Gamma^S \cap \Gamma = \emptyset$.

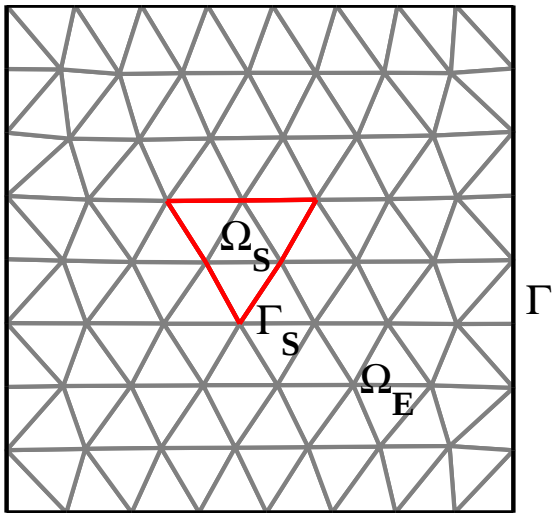

Figure 1: Subdivision of the domain and the mesh. Γ^S is in red.

In Ω^S, we write the field u as the sum of the known field u^I generated by the point source in free space (i.e. with constant parameters ρ^S and κ^S in the whole plane and without any boundary conditions) and the unknown remainder u^S, i.e.

$$u = u^I + u^S \qquad \text{in } \Omega^S, \qquad \text{where} \qquad u^I(\mathbf{x}) := \rho^S \frac{\mathrm{i}}{4} H_0^1(\kappa^S|\mathbf{x} - \mathbf{x}_0|),$$

where H_0^1 is the Hankel function of the first kind and order zero. Then u^I is the fundamental solution of the Helmholtz equation (with constant parameter). By separating out the total field u into the sum of the unknown field and the known local particular solution of the inhomogeneous Helmholtz equation, we can remove the known part, and so are left with the homogeneous form of the equation. We can then use the UWVF to approximate $u^S \in H^1(\Omega^S)$ alone, and add in the known u^I in a post-processing step. In the remainder of the domain Ω^E we approximate the total field u, which we now denote $u^E \in H^1(\Omega^E)$ for clarity.

Since u^I is solution of

$$\nabla \cdot \left(\frac{1}{\rho}\nabla u^I\right) + \frac{\kappa^2}{\rho} u^I = f \qquad \text{in } \Omega^S,$$

and the traces of $(u^S + u^I)$ and u^E should agree on Γ^S, we are left with two homogeneous Helmholtz equations for u^S and u^E, posed in Ω^S and Ω^E respectively, coupled via the impedance traces of u^I:

$$\begin{aligned}
\nabla \cdot \left(\frac{1}{\rho}\nabla u^S\right) + \frac{\kappa^2}{\rho} u^S &= 0 && \text{in } \Omega^S,\\
\nabla \cdot \left(\frac{1}{\rho}\nabla u^E\right) + \frac{\kappa^2}{\rho} u^E &= 0 && \text{in } \Omega^E,\\
(1+Q)\frac{1}{\rho}\frac{\partial u}{\partial n} - (1-Q)\mathrm{i}\sigma u &= g && \text{on } \Gamma,\\
\left(\frac{1}{\rho^S}\frac{\partial}{\partial n_S} - \mathrm{i}\sigma\right) u^S &= \left(-\frac{1}{\rho^E}\frac{\partial}{\partial n_E} - \mathrm{i}\sigma\right) u^E - \left(\frac{1}{\rho^S}\frac{\partial}{\partial n_S} - \mathrm{i}\sigma\right) u^I && \text{on } \Gamma^S,\\
\left(\frac{1}{\rho^E}\frac{\partial}{\partial n_E} - \mathrm{i}\sigma\right) u^E &= \left(-\frac{1}{\rho^S}\frac{\partial}{\partial n_S} - \mathrm{i}\sigma\right) u^S + \left(-\frac{1}{\rho^S}\frac{\partial}{\partial n_S} - \mathrm{i}\sigma\right) u^I && \text{on } \Gamma^S.
\end{aligned} \tag{6}$$

Here, ρ^E is the trace of ρ on Γ^S taken from Ω^E, which does not need to be constant along Γ^S, unlike ρ^S. Recall that on Γ^S we defined $\mathbf{n}_E = -\mathbf{n}_S$, thus the last two conditions in (6) correspond to the continuity of u and $\rho^{-1}\nabla u$ across Γ^S.

The benefit of using the UWVF to approximate $u^S \in H^1(\Omega^S)$ alone is threefold: *(i)* the fields to be approximated are much smoother than the solution of the original problem; *(ii)* they are solution of the homogeneous Helmholtz equation, thus the approximation by Trefftz functions can deliver great accuracy; and *(iii)* all the terms that will appear at the right-hand side of the UWVF are integrals on some part of the mesh skeleton (see equation (8) below).

In the case of a domain of constant wavenumber it would be possible to approximate u^S only on the whole domain (i.e., to choose $\Omega^S = \Omega$, $\Omega^E = \emptyset$, and solve a BVP whose trace source g is modified by subtracting a trace of u^I). However, if the wavenumber is varying in the domain, it is unlikely that a special solution u^I would be known in the whole of Ω.

As in Section 2, if we follow the proof of [5, Theorem 1.3] and insert the last two conditions of (6) in (4), we obtain the ultra weak variational formulation of the BVP (6) as

$$\text{seek } u^* \in H \text{ s.t.} \qquad d(u^*, w) - c(u^*, w) = \beta(w) \qquad \forall w \in H, \tag{7}$$

where u^* stands for u^S and u^E in Ω^S and Ω^E respectively. The sesquilinear forms $d(\cdot,\cdot)$ and $c(\cdot,\cdot)$ were defined in (2) and the antilinear functional $\beta : H \to \mathbb{C}$ is defined as

$$\begin{aligned}\beta(w) := &\sum_{k=1}^{K} \int_{\Gamma_k} \frac{g}{\sigma} \overline{\left(\frac{1}{\rho_k}\frac{\partial}{\partial n_k} - \mathrm{i}\sigma\right) w_k}\,\mathrm{d}S \\ &- \sum_{\Omega_k \in \mathcal{T}^S} \int_{\partial\Omega_k \cap \Gamma^S} \frac{1}{\sigma}\left(\frac{1}{\rho^S}\frac{\partial}{\partial n_S} - \mathrm{i}\sigma\right) u^I \overline{\left(\frac{1}{\rho^S}\frac{\partial}{\partial n_S} - \mathrm{i}\sigma\right) w_k}\,\mathrm{d}S \\ &+ \sum_{\Omega_k \in \mathcal{T}^E} \int_{\partial\Omega_k \cap \Gamma^S} \frac{1}{\sigma}\left(-\frac{1}{\rho^S}\frac{\partial}{\partial n_S} - \mathrm{i}\sigma\right) u^I \overline{\left(\frac{1}{\rho^E}\frac{\partial}{\partial n_E} - \mathrm{i}\sigma\right) w_k}\,\mathrm{d}S \qquad \forall w \in H.\end{aligned} \tag{8}$$

The discrete version of the UWVF read as follows: given a finite dimensional subspace $H_h \subset H$,

$$\text{seek } u_h^* \in H_h \text{ s.t.} \qquad d(u_h^*, w_h) - c(u_h^*, w_h) = \beta(w_h) \qquad \forall w_h \in H_h. \tag{9}$$

The corresponding linear system of equations has the same matrix as the system obtained from the standard UWVF (3), while the right-hand side vector is different. The system reads $(D - C)X = b$, where X is the coefficient vector of u_h^* in a given basis of H_h. The matrix D is Hermitian and block diagonal (with blocks D_k of size p_k, for $k = 1, \ldots, K$), with each entry given by an integral over the boundary of an element; each entry of the sparse matrix C contains two integrals over edges; see [11, Section 3] for more details.

3.1 Well-posedness of the Source Extraction UWVF

We define the trace space $X := \prod_{k\in K} L^2(\partial\Omega_k)$, equipped with the norm

$$\|\mathcal{X}\|_X^2 := \sum_{k=1}^{K} \int_{\partial\Omega_k} \frac{1}{\sigma} |\mathcal{X}_k|^2 \,\mathrm{d}S \qquad \forall \mathcal{X} = (\mathcal{X}_1, \ldots \mathcal{X}_K) \in X.$$

In the space X we define the impedance and the "adjoint impedance" trace operators

$$\mathcal{I} : H \to X, \qquad F : \mathcal{I}(H) \to X$$

as

$$\mathcal{I}(v) := \big(\mathcal{I}_1(v), \dots, \mathcal{I}_K(v)\big), \qquad \mathcal{I}_k(v) := -\frac{1}{\rho_k}\frac{\partial v_k}{\partial n} - i\sigma v_k \quad \text{and}$$

$$F\big(\mathcal{I}(v)\big) := \Big(F_1\big(\mathcal{I}_1(v)\big), \dots, F_K\big(\mathcal{I}_K(v)\big)\Big), \qquad F_k\big(\mathcal{I}_k(v)\big) := \frac{1}{\rho_k}\frac{\partial v_k}{\partial n} - i\sigma v_k.$$

Then the UWVF sesquilinear form (3) may immediately be rewritten as

$$\begin{aligned} d(u,v) - c(u,v) = \sum_{k=1}^{K} \Bigg[& \int_{\partial\Omega_k} \frac{1}{\sigma}\mathcal{I}_k(u)\overline{\mathcal{I}_k(v)}\,\mathrm{d}S \\ & - \sum_{\substack{j=1 \\ j\neq k}}^{K} \int_{\Sigma_{j,k}} \frac{1}{\sigma}\mathcal{I}_j(u)\overline{F_k\big(\mathcal{I}_k(v)\big)}\,\mathrm{d}S - \int_{\Gamma_k} \frac{Q}{\sigma}\mathcal{I}_k(u)\overline{F_k\big(\mathcal{I}_k(v)\big)}\,\mathrm{d}S \Bigg]. \end{aligned}$$

Buffa and Monk defined in [3, (2.16)] the sesquilinear form $a : X \times X \to \mathbb{C}$

$$a(\mathcal{X}, \mathcal{Y}) := \frac{1}{2}\big(d(u,v) - c(u,v)\big) \qquad \text{for } u, v \in H \text{ s.t. } \mathcal{I}(u) = \mathcal{X},\ \mathcal{I}(v) = \mathcal{Y}$$

in the case $Q = 0$. The form $a(\cdot,\cdot)$ is well-defined, as there exists a unique $u \in H$ satisfying $\mathcal{I}(u) = \mathcal{X} \in X$ by the well-posedness of the corresponding Helmholtz impedance BVPs posed in the mesh elements. In other words $\mathcal{I} : H \to X$ is invertible. Note that in [3] κ is taken constant, $\rho = 1$, η is used in place of σ and the relationship between $\mathcal{X}$ and u (and similarly between $\mathcal{Y}$ and v) follows a different sign convention.

Lemma 3.4 of [3] provides the coercivity of $a(\cdot,\cdot)$ when $Q = 0$. The applicability of this result to the present setting can be verified by defining $\mathbf{v} := (-\mathrm{i}\rho)^{-1}\nabla u$, $\mathcal{X}_k := (-\mathrm{i}\sigma u_k + \mathrm{i}\mathbf{v}_k \cdot \mathbf{n}_k) \in L^2(\partial\Omega_k)$ and repeating exactly the same proofs of [3] with a different sign convention; the discontinuous coefficients do not affect this result. From this, both the continuous and the discrete problems (7) and (9) are well-posed. We have the following error bound for the discretisation of the UWVF which was proved in [3, Theorem 3.5]:

$$\begin{aligned} & \sum_{j,k=1}^{K} \int_{\Sigma_{j,k}} \left(\frac{\sigma}{2}\big|[\![u^* - u_h^*]\!]\big|^2 + \frac{1}{2\sigma}\left|\left[\!\!\left[\frac{1}{\rho}\nabla u^* - \nabla u_h^*\right]\!\!\right] \cdot \mathbf{n}\right|^2 \right) \mathrm{d}S \\ & + \sum_{k} \int_{\Gamma_k} \frac{1}{2\sigma}\Big(\Big|F_k\big(\mathcal{I}_k(u^*)\big) - F_k\big(\mathcal{I}_k(u_h^*)\big)\Big|^2 + \Big|\mathcal{I}_k(u^*) - \mathcal{I}_k(u_h^*)\Big|^2 \Big) \mathrm{d}S \end{aligned}$$

$$\leq 4 \inf_{v_h \in H_h} \|\mathcal{I}(u^*) - \mathcal{I}(v_h)\|_X^2 , \tag{10}$$

where $[\![\cdot]\!]$ denotes the jumps across the mesh faces Σ_{jk}.

This bound allows us to control the traces of the error on the mesh skeleton only. Theorem 4.1 of [3] then gives an error estimate in the $L^2(\Omega)$-norm, but holds for BVPs with $H^2(\Omega)$-regularity only: since here we consider discontinuous coefficients, it is not directly applicable in the present case. In order to obtain estimates in $L^2(\Omega)$, a new duality result similar to Lemma 4.4 of [10] (which improves on [3, Theorem 4.1] in requiring weaker regularity than $H^2(\Omega)$) is required.

Given a particular discrete Trefftz space, in order to obtain orders of convergence from the quasi-optimality bound (10), only best-approximation estimates are needed. In the case of plane wave or Fourier–Bessel (i.e. circular waves) basis, these approximation bounds are proved and discussed in [16].

4 Numerical examples

We present two numerical examples of the Source Extraction UWVF described in Section 3 for solving the inhomogeneous Helmholtz equation (1a). In the first we consider the approximation of the wave generated by a point source in a domain of constant wave speed, and compare the accuracy with that of the original formulation. In the second example we consider the suitability of the Source Extraction UWVF for seismic imaging applications, testing on a wave speed profile given by a synthetic seismic model.

We solve the inhomogeneous Helmholtz problem (1) with a point source as in (5). In both examples we use a constant density $\rho = 1$ over the domain, while we take the wavenumber κ to be constant in the first example and discontinuous in the second one. We fix $Q = 0$ in the impedance boundary condition (1b). The source region Ω^S is defined to comprise four triangular elements: that containing the point source and its three neighbours (see Figure 1).

The Trefftz basis functions $\phi_{k,l} \in H_k$ used are Hankel functions, defined as

$$\phi_{k,l}(\mathbf{x}) = \begin{cases} H_0^1(\kappa_k |\mathbf{x} - \mathbf{y}_{k,l}|) & \text{in } \Omega_k, \\ 0 & \text{elsewhere,} \end{cases} \tag{11}$$

for $l = 1, ..., p_k$, $k = 1, ..., K$. Their centres $\mathbf{y}_{k,l}$ are equispaced and located externally to the respective elements:

$$\mathbf{y}_{k,l} = \left(x_k^C + R \cos\left(\frac{2\pi l}{p_k}\right), y_k^C + R \sin\left(\frac{2\pi l}{p_k}\right) \right), \qquad l = 1, ..., p_k.$$

Here $R > d_{\max} > 0$ is a positive constant greater than the maximum distance $d_{max} = \max_s(|\mathbf{x}_k^C - \mathbf{x}_{k,s}^V|)$ between the centroid of the element $\mathbf{x}_k^C = (x_k^C, y_k^C)$ and each vertex $\mathbf{x}_{k,s}^V$ of Ω_k, $s = 1, 2, 3$. The Hankel basis permits flexibility in the choice of the propagation direction and the curvature of wavefronts. These basis functions approximate the conventional plane waves if the points $\mathbf{y}_{k,l}$ lie in the far field (i.e. for large values of R), whereas by taking $\mathbf{y}_{k,l}$ closer to Ω_k the wavefront curvature is increased. The UWVF integrals in (2) and (8) cannot be evaluated in closed form, so a numerical integration method is required. We use a Gauss–Legendre quadrature rule, with forty points per wavelength for high accuracy, allowing us to focus on the effects of the Source Extraction UWVF.

In each simulation, an initial maximum number p of basis functions per element is set, then p_k is reduced if the condition number of the submatrix D_k is above a set tolerance level of 10^{10}: this scheme was first introduced in [11]. More details about the effect of the number of basis functions and the element size on the conditioning of D_k can be found in [5, 11, 14].

4.1 Interior point source in a domain with constant parameters

For the first example we consider a square domain $\Omega = (0, 3) \times (0, 3)$ in which the wavenumber is constant throughout. In order to focus just on the accuracy of the Source Extraction UWVF, the boundary condition (1b) (with $Q = 0$) was set to impose as exact solution of the BVP the fundamental solution of the Helmholtz equation,

$$u(\mathbf{x}) = \frac{\mathrm{i}}{4} H_0^1(\kappa|\mathbf{x} - \mathbf{x}_0|), \tag{12}$$

with $\mathbf{x}_0 = (1.40, 1.60) \in \Omega$. We approximate this solution using both the classical UWVF (3) and the Source Extraction UWVF described in Section 3. An example solution of the Source Extraction UWVF is shown in Figure 2 for $\kappa = 10$, along with the computational mesh of $K = 116$ elements; this approximation was achieved using $p = 15$ basis functions on each element. Table 1 shows the relative error, measured in the $L^2(\Omega)$-norm, for the two methods, together with the average number N_λ of degrees of freedom per wavelength in each direction, computed as

$$N_\lambda = \lambda \sqrt{\frac{\sum_{k=1}^K p_k}{|\Omega|}},$$

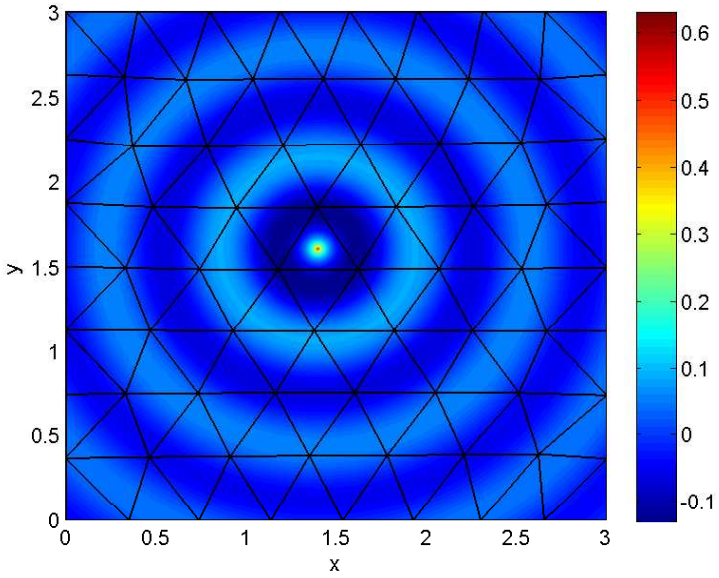

Figure 2: The real part of the the inhomogeneous Helmholtz problem with constant coefficients for $\kappa = 10$, approximated using the Source Extraction UWVF on $K = 116$ elements by $p = 15$ basis functions per element. The computational mesh is superimposed.

where $|\Omega|$ is the area of the domain. The Source Extraction UWVF provides a much higher accuracy than the classical formulation for the same approximation parameters K and p. In all cases it was not necessary to reduce p_k to maintain the condition number bound, so $p_k = p$ for $k = 1, ..., K$.

The accuracy obtained by the Source Extraction UWVF for this BVP is comparable to that achieved by the classical formulation of the UWVF when solving the homogeneous Helmholtz equation ($f = 0$) for a BVP whose exact solution is a fundamental solution centred outside the domain Ω (i.e. u as in (12) with $\mathbf{x}_0 \notin \Omega$); see Table 2 for the UWVF error in this setting.

The plot in Figure 3 shows that accurate results can be achieved for various wavenumbers using the Source Extraction UWVF for approximating an interior point source problem. As expected, computations with the fundamental solution centred at $\mathbf{x}_0$ used as one of the basis functions gave results accurate to machine precision, even when using elements several wavelengths in width.

p	$L^2(\Omega)$ relative error, classical UWVF	$L^2(\Omega)$ relative error, Source Extraction UWVF	N_λ
9	4.6148×10^{-1}	9.8941×10^{-3}	6.7672
10	4.6138×10^{-1}	5.2901×10^{-3}	7.1332
11	4.6087×10^{-1}	1.5578×10^{-3}	7.4814
12	4.6159×10^{-1}	8.2696×10^{-4}	7.8140
13	4.6154×10^{-1}	3.3895×10^{-4}	8.1331
14	4.6151×10^{-1}	2.2961×10^{-4}	8.4401
15	4.6145×10^{-1}	8.5399×10^{-5}	8.7364
16	4.6145×10^{-1}	6.5757×10^{-5}	9.0229

Table 1: Errors of the classical and the Source Extraction UWVF measured in $L^2(\Omega)$-norm for a point source in the interior of a homogeneous domain. Approximation by p equally spaced point sources per element, $K = 116$, $\kappa = 10$, $\Omega = (0, 3) \times (0, 3)$.

p	$L^2(\Omega)$ relative error, classical UWVF	N_λ
10	5.6961×10^{-3}	7.1332
11	1.1964×10^{-3}	7.4814
12	8.6834×10^{-4}	7.8140
13	1.7065×10^{-4}	8.1331
14	9.6792×10^{-5}	8.4401
15	1.8955×10^{-5}	8.7364

Table 2: Errors of the classical formulation measured in $L^2(\Omega)$-norm for the homogeneous Helmholtz equation: the exact solution is a fundamental solution centred at $(-0.5, 1.5)$ in the exterior of the domain. Approximation by p equally spaced point sources per element, $K = 116$, $\kappa = 10$, $\Omega = (0, 3) \times (0, 3)$.

4.2 Interior point source in a section of a smoothed Marmousi model

We now progress to testing the method on a domain more relevant to seismic imaging, where the sound speed is non-constant. The synthetic Marmousi model is a 2D representation of typical geophysical structures in the sub-surface of the Earth, widely used as a test problem in seismic imaging [15]. The domain Ω is taken as a section of a smoothed Marmousi sound speed

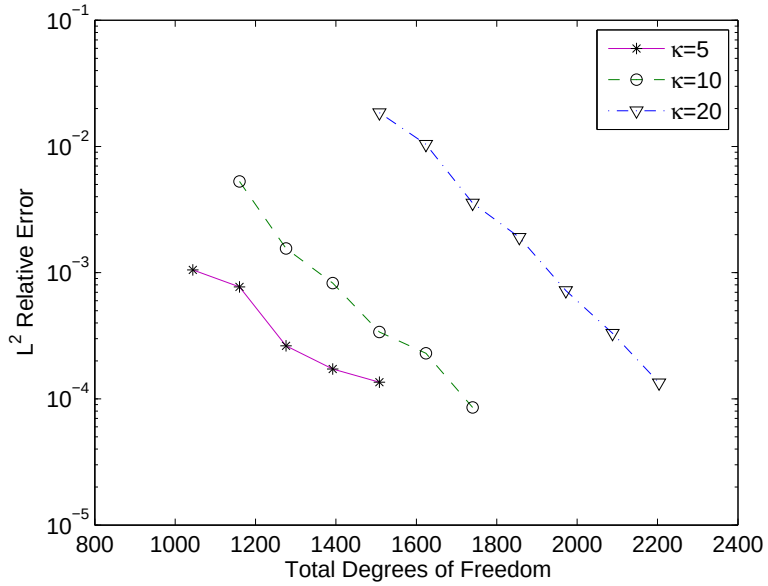

Figure 3: Relative $L^2(\Omega)$ errors against total number of degrees of freedom for the inhomogeneous Helmholtz problem with constant coefficients, approximated using the Source Extraction UWVF on $K = 116$ elements in $\Omega = (0,3) \times (0,3)$. For $\kappa = 5$ we consider $p = 9, \ldots, 13$, for $\kappa = 10$ $p = 10, \ldots, 15$, and for $\kappa = 20$ $p = 13, \ldots, 19$.

profile, that of $x \in (3.5131, 7.0022)$ km, $z \in (0, 2.0565)$ km, as shown in the upper plot of Figure 4. As we use a constant density $\rho = 1$ throughout, the only discontinuous parameter in the discretisation of the domain is the wavenumber κ.

For the Source Extraction UWVF approximation, two levels of mesh refinements are used, resulting in $K = 485$ and $K = 771$ triangular elements. The point source is located in $\mathbf{x}_0 = (6.018, 0.5768)$ and lies in the interior of an element, thus we avoid the case of the solution singularity coinciding with element edges or vertices. In order to explore just the accuracy associated with source extraction, a simple homogeneous impedance condition is imposed on the boundary (1b with $Q = 0$ and $g = 0$).

To obtain a piecewise-constant wavenumber, for each $\Omega_k \in \mathcal{T}^E$, $\kappa|_{\Omega_k} = \kappa_k$ is taken to be the average of the wavenumber of the smoothed Marmousi model at the three vertices of the element. In Ω^S the wavenumber is constant, taken as the average of values interpolated at the centre of each $\Omega_k \in \Omega^S$. The centre and lower plots of Figure 4 show the two meshes used, the discretised

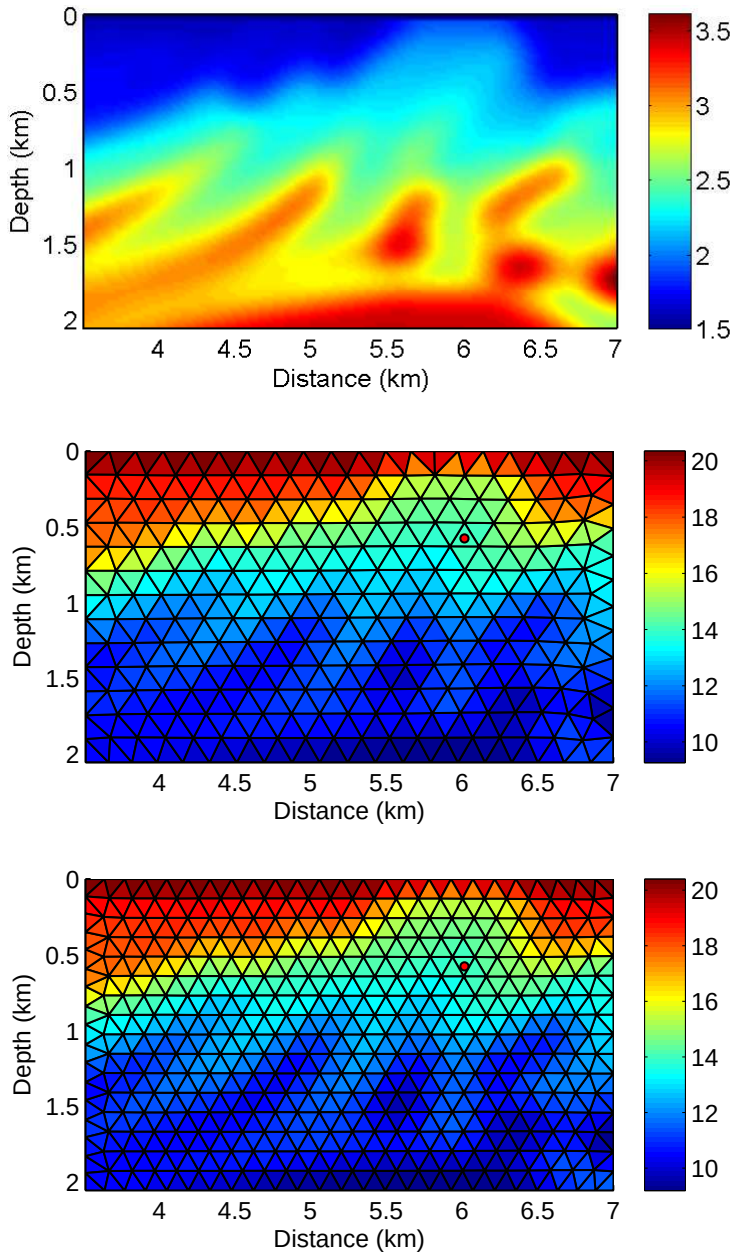

Figure 4: Upper plot: wave speed (km/s) in a section of the smoothed Marmousi model. Centre and lower plots: wavenumber κ_k in each element of the discretisation of the above velocity profile for the frequency 5 Hz, using $K = 485$ elements (centre plot) and $K = 771$ elements (lower plot). (Recall that $\kappa = 2\pi \cdot$frequency/wave speed.) The point source location is marked by a red dot.

(piecewise constant) wavenumber for a frequency of 5 Hz and the position of the point source. The same discretisations are used for the frequency 10 Hz, resulting in the wavenumber in each element being doubled.

The angularly equispaced basis (11) is used, with $R = 100$ to replicate the conventional plane wave basis. An initial maximum number $p = 15$ of basis functions per element is set, and then p_k reduced if the condition number of the submatrix D_k is above the tolerance level of 10^{10}. The range of values taken by p_k across the mesh and the total number of degrees of freedom obtained for the frequencies 5 and 10 Hz and for the two meshes is summarised in Table 3.

Frequency	K	Range of p_K	Total number of degrees of freedom
5 Hz	485	[8,...,15]	5,162
5 Hz	771	[8,...,13]	6,636
10 Hz	485	[11,...,15]	7,417
10 Hz	771	[10,...,15]	9,749

Table 3: The range of the values taken by the local number of degrees of freedom p_k and the total number of degrees of freedom $\sum_{k=1}^{K} p_k$ obtained with the adaptive procedure for the frequencies 5 and 10 Hz and for the two meshes with 485 and 771 triangles shown in Figure 4.

The upper and centre plots of Figure 5 show the real part of the Source Extraction UWVF solution for the frequency 5 Hz and for the discretisations with $K = 485$ and $K = 771$ elements, respectively. The lower plot shows the real part of a reference solution computed with a finite difference scheme for comparison. (This was obtained on a regular structured grid with 180 points per wavelength and using the method described in [8].) Figure 6 shows results in the same setup for the frequency 10 Hz. In both cases, the general pattern and areas of heightened or dampened amplitudes do coincide.

5 Conclusions

We have considered the use of the UWVF for solving the inhomogeneous Helmholtz equation in the special case of a point source. The UWVF typically has problems when the Trefftz basis functions do not well represent the inhomogeneity of the equation. To avoid the use of alternative numerical methods in the region of inhomogeneity, we propose an augmentation of the UWVF equations called the Source Extraction UWVF. This technique requires only a homogeneous equation to be solved, with inhomogeneity introduced in a post-processing step, thus it better exploits the Trefftz property

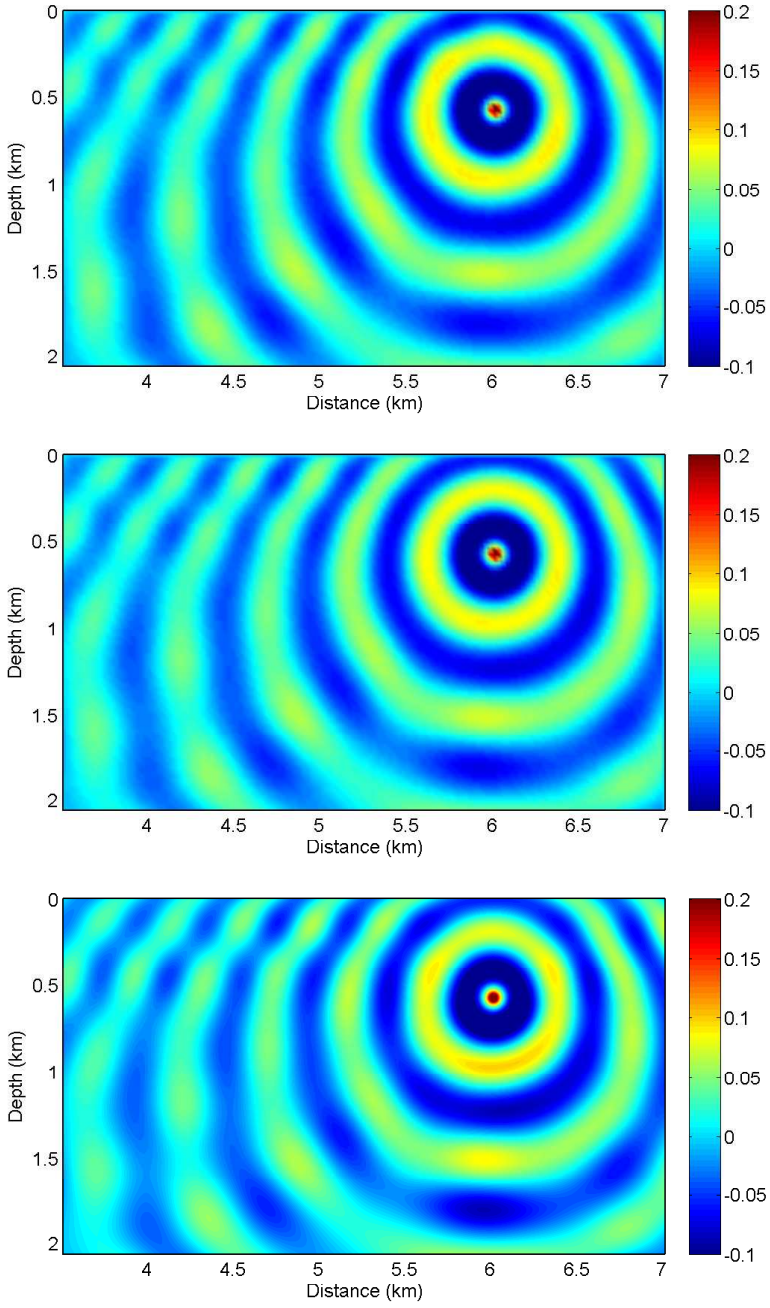

Figure 5: Real part of the total field approximation in the smoothed Marmousi section with frequency 5 Hz: UWVF solution with $K = 485$ and $\max_k p_k = 15$ (upper plot), UWVF solution with $K = 771$ and $\max_k p_k = 13$ (centre plot), finite difference solution (lower plot).

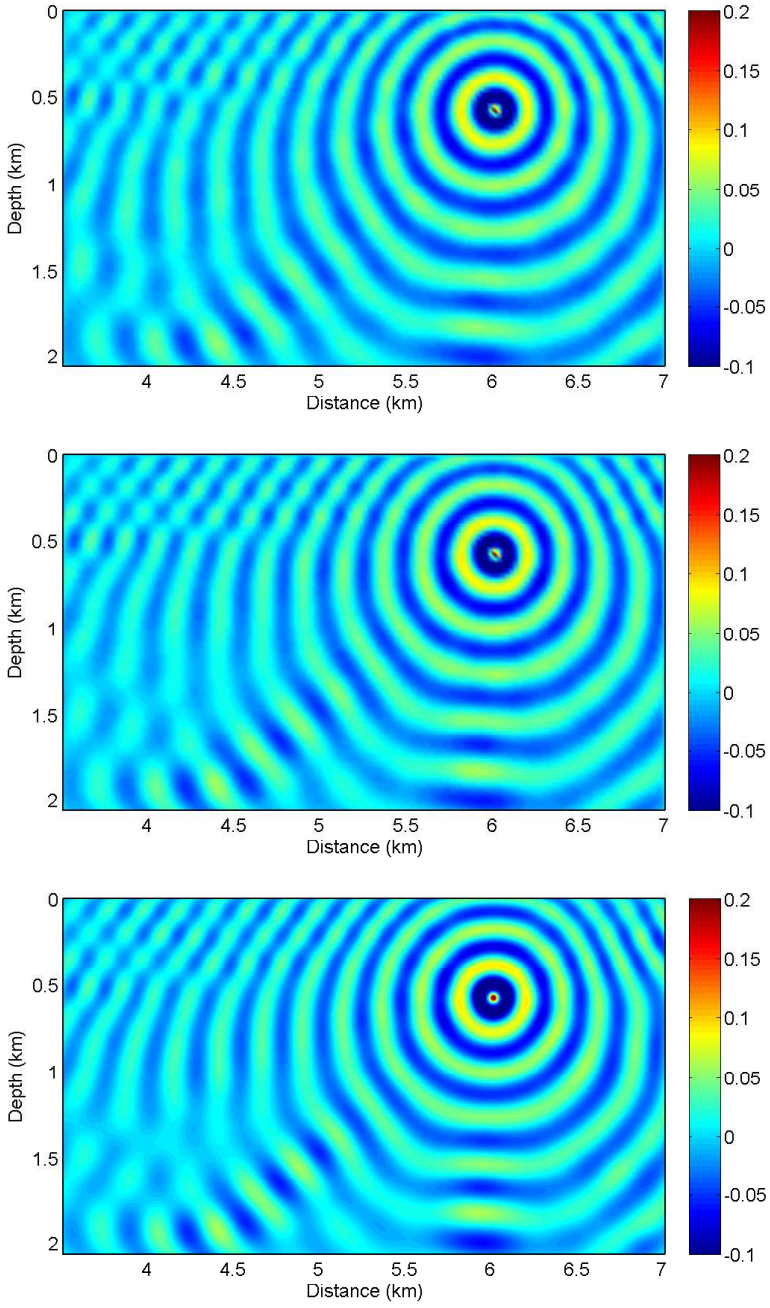

Figure 6: Real part of the total field approximation in the smoothed Marmousi section with frequency 10 Hz: UWVF solution with $K = 485$ and $\max_k p_k = 15$ (upper plot), UWVF solution with $K = 771$ and $\max_k p_k = 15$ (centre plot), finite difference solution (lower plot).

of the discrete space. For a point source, we approximate the unknown back-scattered field in a region surrounding the source, and match this to the total field approximated in the remainder of the domain. In the considered examples we use a Dirac delta point source; however, the augmentation of the method can be easily generalised to other forms of source function, such as dipoles and multipoles. Following on from work in [3], we show that the Source Extraction UWVF is well-posed and satisfies the error bound (10) on the mesh skeleton in the case of impedance boundary conditions and sufficiently smooth solution. Numerical simulation has shown that the Source Extraction UWVF is much more accurate than the classical UWVF for the approximation of interior point sources. The method is also used to provide simulation of wave scattering in a sound speed profile typical of seismic imaging applications. Results presented concur with those of a finite difference method.

References

[1] R. Abgrall and J. Benamou. Big ray-tracing and eikonal solver on unstructured grids: Application to the computation of a multivalued traveltime field in the Marmousi model. *GEOPHYSICS*, 64(1):230–239, 1999.

[2] Z. Alterman and F. Karal. Propagation of elastic waves in layered media by finite difference methods. *Bulletin of the Seismological Society of America*, 58(1):367–398, 1968.

[3] A. Buffa and P. Monk. Error estimates for the ultra weak variational formulation of the Helmholtz equation. *ESAIM: Mathematical Modelling and Numerical Analysis*, 42:925–940, 2008.

[4] O. Cessenat. *Application d'une nouvelle formulation variationnelle aux équations d'ondes harmoniques. Problèmes de Helmholtz 2D et de Maxwell 3D.* PhD thesis, Paris IX Dauphine, 1996.

[5] O. Cessenat and B. Després. Application of an ultra weak variational formulation of elliptic PDEs to the two-dimensional Helmholtz problem. *SIAM Journal on Numerical Analysis*, 35(1):255–299, 1998.

[6] G. Gabard. Discontinuous Galerkin methods with plane waves for time-harmonic problems. *Journal of Computational Physics*, 225(2):1961 – 1984, 2007.

[7] C. J. Gittelson, R. Hiptmair, and I. Perugia. Plane wave discontinuous Galerkin methods: Analysis of the h-version. *ESAIM: Mathematical Modelling and Numerical Analysis*, 43:297–331, 3 2009.

[8] I. Harari and E. Turkel. Accurate finite difference methods for time-harmonic wave propagation. *J. Comp. Phys.*, 119:252–270, 1995.

[9] R. Hiptmair, A. Moiola, and I. Perugia. Plane wave discontinuous Galerkin methods for the 2D Helmholtz equation: Analysis of the p-version. *SIAM Journal on Numerical Analysis*, 49(1):264–284, 2011.

[10] R. Hiptmair, A. Moiola, and I. Perugia. Trefftz discontinuous Galerkin methods for acoustic scattering on locally refined meshes. *Applied Numerical Mathematics*, to appear, 2013.

[11] T. Huttunen, P. Monk, and J. P. Kaipio. Computational aspects of the ultra-weak variational formulation. *Journal of Computational Physics*, 182(1):27–46, 2002.

[12] M. Loeser and B. Witzigmann. The ultra weak variational formulation applied to radiation problems with macroscopic sources in inhomogeneous domains. *Selected Topics in Quantum Electronics, IEEE Journal of*, 15(4):1144–1155, 2009.

[13] T. Luostari, T. Huttunen, and P. Monk. The ultra weak variational formulation using Bessel basis functions. *Communications in Computational Physics*, 11(2):400–414, 2012.

[14] T. Luostari, T. Huttunen, and P. Monk. Improvements for the ultra weak variational formulation. *International Journal for Numerical Methods in Engineering*, 94(6):598–624, 2013.

[15] G. S. Martin, R. Wiley, and K. J. Marfurt. Marmousi2: An elastic upgrade for Marmousi. *The Leading Edge*, 25(2):156–166, 2006.

[16] A. Moiola, R. Hiptmair, and I. Perugia. Plane wave approximation of homogeneous Helmholtz solutions. *Zeitschrift für Angewandte Mathematik und Physik (ZAMP)*, 62:809–837, 2011.

[17] I. Opršal, C. Matyska, and K. Irikura. A general boundary condition in 3D hybrid wave injection modeling based on Alterman and Karal (1968) method. *Proc. 14 World Conf. Earthq. Eng.*, 2008.